E-sail Attitude Control with Tether Voltage Modulation

M. Bassetto*, L. S. Álvarez Mera†, G. Mengali‡, and A. A. Quarta§
Department of Civil and Industrial Engineering, University of Pisa, Italy, I-56122

The Electric Solar Wind Sail (E-sail) is a propellantless propulsion system that gains thrust from the interaction of solar wind particles with a grid of long charged tethers, which are deployed by spinning the spacecraft about a symmetry axis. In an ideal situation, the tethers are perfectly stretched and the E-sail takes the shape of a rigid disk. Actually, the solar wind dynamic pressure warps the tethers and, therefore, the expressions of the thrust and torque vectors are difficult to predict. Recent works have shown that the bending of the tethers induces a disturbance torque, which can be counterbalanced through a modulation of the tether electrical voltage. Under the assumption that the E-sail behaves like an axially-symmetric rigid body, this paper proves that the modulation of the tether electrical voltage is a promising option for controlling and maintaining the spacecraft attitude. The proposed control law, which is analytically provided as a function of time and current sail attitude, is validated through numerical integration of the attitude dynamic equations.

Nomenclature

A	=	constant; see Eq. (17), [rad/s]
b_l	=	dimensionless shape coefficient; see Eq. (5)
$\mathrm{d}s$	=	elementary length of tether, [m]
$\mathcal{E}$, $\mathcal{F}$, $\mathcal{G}$	=	components of E-sail torque in $\mathcal{T}_B$, [N m]
f	=	distance of $\mathrm{d}s$ from $(x_B,\ y_B)$ plane; see Eq. (4), [m]
$\boldsymbol{F}_t$	=	projection of thrust vector on $(x_B,\ y_B)$ plane, [N]
$\boldsymbol{H}$	=	spacecraft angular momentum vector, [kg m^2/s]
I_t	=	transverse moment of inertia, [kg m^2]
I_z	=	longitudinal moment of inertia, [kg m^2]
$\hat{\boldsymbol{i}}_A$, $\hat{\boldsymbol{j}}_A$, $\hat{\boldsymbol{k}}_A$	=	unit vectors of $\mathcal{T}_A$
$\hat{\boldsymbol{i}}_B$, $\hat{\boldsymbol{j}}_B$, $\hat{\boldsymbol{k}}_B$	=	unit vectors of $\mathcal{T}_B$
$\hat{\boldsymbol{i}}_I$, $\hat{\boldsymbol{j}}_I$, $\hat{\boldsymbol{k}}_I$	=	unit vectors of $\mathcal{T}_I$
L	=	tether length, [m]
m_p	=	proton mass, [kg]
N	=	number of tethers
n	=	solar wind number density, [m^{-3}]
$\hat{\boldsymbol{r}}$	=	Sun-spacecraft unit vector
S	=	spacecraft center-of-mass
t	=	time, [s]
$\boldsymbol{T}_a$	=	attitude variation torque (with $T_a \triangleq \|\boldsymbol{T}_a\|$), [N m]
$\boldsymbol{T}_c$	=	control torque (with $T_c \triangleq \|\boldsymbol{T}_c\|$); see Eq. (22), [N m]
$\boldsymbol{T}_d$	=	disturbance torque (with $T_d \triangleq \|\boldsymbol{T}_d\|$), [N m]
t_f	=	attitude maneuver time, [s]
$\mathcal{T}_A$	=	auxiliary reference frame
$\mathcal{T}_B$	=	principal body reference frame
$\mathcal{T}_I$	=	inertial reference frame

*Ph.D. student, Department of Civil and Industrial Engineering, University of Pisa, Via Caruso 8, Pisa, Italy, marco.bassetto@ing.unipi.it
†Graduate student, lau.alvarezmera@gmail.com
‡Professor, Department of Civil and Industrial Engineering, University of Pisa, Via Caruso 8, Pisa, Italy, g.mengali@ing.unipi.it
§Professor, Department of Civil and Industrial Engineering, University of Pisa, Via Caruso 8, Pisa, Italy, a.quarta@ing.unipi.it

u = solar wind speed, [m/s]
V = tether electric potential, [V]
V_w = solar wind electric potential, [V]
x = curvilinear abscissa, [m]
x_A, y_A, z_A = axes of $\mathcal{T}_A$
x_B, y_B, z_B = axes of $\mathcal{T}_B$
x_I, y_I, z_I = axes of $\mathcal{T}_I$
α_n = pitch angle; see Eq. (2), [rad]
β = angle between the control plane and x_A-axis; see Eq. (24), [rad]
γ_k = angle between the k-th tether and x_A-axis; see Eq. (25), [rad]
δ_n = clock angle; see Eq. (3), [rad]
ϵ_0 = vacuum permittivity, [F/m]
ζ_k = angular position of the k-th tether; see Eq. (1), [rad]
λ = ratio, see Eq. (12)
ρ = tether linear mass density, [kg/m]
σ = design parameter; see Eq. (6), [kg/m/s]
ϕ, θ, ψ = Euler's angles, [rad]
ω = nominal sail spin rate, [rad/s]
$\mathbf{\Omega}$ = spacecraft angular velocity, [rad/s]
$\mathbf{\Omega}_A$ = angular velocity of $\mathcal{T}_A$, [rad/s]
Ω_x, Ω_y, Ω_z = components of $\mathbf{\Omega}$ in $\mathcal{T}_B$, [rad/s]

Subscripts

f = final
k = referred to the k-th tether
max = maximum
min = minimum

Superscripts

$'$ = derivative with respect to x
$\dot{}$ = derivative with respect to t
$\tilde{}$ = expected value

1. Introduction

An Electric Solar Wind Sail (E-sail) is a propellantless propulsion system [1, 2] that gains thrust from the interaction of solar wind particles with a grid of long charged tethers, which are kept at a high voltage level by means of an electron emitter [3]. The tethers are deployed and maintained ideally stretched by spinning the spacecraft about its symmetry axis [4–6]. In such a special situation, the E-sail takes the shape of a rigid disk [7], and the propulsive acceleration may be described with the analytical model by Huo et al. [8]. In particular, Ref. [8] shows that the E-sail does not generate any torque when the tethers are straight and the electrical voltage is uniform. Their actual shape, however, is not so plain, as it comes out from the chaotic interaction between the solar wind dynamic pressure and the centrifugal force due to the spacecraft rotation. The uncertainty associated with the actual shape of each tether complicates an estimate of the thrust and torque vectors, which are necessary information for preliminary mission analysis and trajectory simulation.

Recent works [9, 10] have addressed the problem of providing approximate closed-form expressions of the E-sail thrust and torque vectors. In particular, the results reported in Ref. [9], based on the assumption of a Sun-facing sail [11, 12], show that the tether equilibrium shape is well approximated by a natural logarithmic arc when the spacecraft spin rate is sufficiently high. However, in a Sun-facing configuration the E-sail generates a purely radial thrust, while in most cases a trasverse thrust component is necessary for orbital maneuvers, as it allows the angular momentum to be varied. Typical missions include the design of linear [13] or displaced [14, 15] trajectories, interplanetary rendezvous [16–22], or the exploration of the outer Solar System [23–25]. Such a transverse thrust component may be

obtained by inclining the sail plane with respect to the local radial direction. However, the tethers' bending causes the onset of a disturbance torque [10] that induces a perturbation on the orientation of the spin axis. The latter experiences an undamped precession-nutation motion, which eventually tends to align the thrust vector along the Sun-spacecraft direction. A possible solution to this problem is discussed in Ref. [26], where it is shown that the disturbance torque may be removed with a modulation of the tether electrical voltage, without affecting the total thrust.

The aim of this paper is to propose a new strategy for controlling and maintaining the E-sail attitude. Previous works on this subject begin with Ref. [27], in which Janhunen has discussed the problem of creating and modifying the E-sail spin rate with small photonic sails applied to the tips of the main tethers. Later, Toivanen and Janhunen [28] have shown that the sail attitude can be controlled by modulating the voltage of each individual tether to produce a torque for thrust vectoring, and in Ref. [29] they have also suggested to modulate the tether voltage synchronously with the sail rotation. Finally, Janhunen and Toivanen [30] have recently presented an algorithm to control the sail attitude, in which the tethers are modeled as elastic wires, while the solar wind properties are taken from historical satellite data. In the present paper the control is obtained by modulating the electrical voltage of each individual tether as a function of time and current sail attitude, assuming that the sail maintains an axially-symmetric shape. In particular, the E-sail is virtually divided in two parts, each one characterized by a precise level of electrical voltage. To that end, a control plane is defined [26], which is used to locate where the tether voltage must be varied with respect to its nominal value. The control plane is perpendicular to the sail nominal plane, and its angular position is used in the control law. The amplitude of the voltage modulation is obtained in an indirect way by enforcing the sail attitude to track a desired time evolution. The control strategy is validated through a numerical simulation, which shows that the required torque may actually be generated with a small modulation of the electrical voltage with respect to its reference value.

The paper is organized as follows. Section 2 introduces the mathematical model used to describe both the sail geometry and the disturbance torque vector. Section 3 deals with the derivation of the analytical control law, while Section 4 illustrates its effectiveness and quantifies its performance. Some concluding remarks are given in the last section.

2. Mathematical preliminaries

2.1 Geometrical model

To a first-order approximation, the spacecraft (including the E-sail) is modeled as an axially-symmetric rigid body. Its shape resembles that of a large spoked wheel, in which each spoke is substituted by a tether. All of the tethers ideally belong to the same plane, referred to as sail nominal plane. Introduce a principal body reference frame $\mathcal{T}_B(S;\, x_B,\, y_B,\, z_B)$ of unit vectors $\{\hat{\boldsymbol{i}}_B,\, \hat{\boldsymbol{j}}_B,\, \hat{\boldsymbol{k}}_B\}$, where $\hat{\boldsymbol{k}}_B$ is aligned with the spacecraft symmetry axis, while $(x_B,\, y_B)$ coincides with the E-sail nominal plane; see Fig. 1.

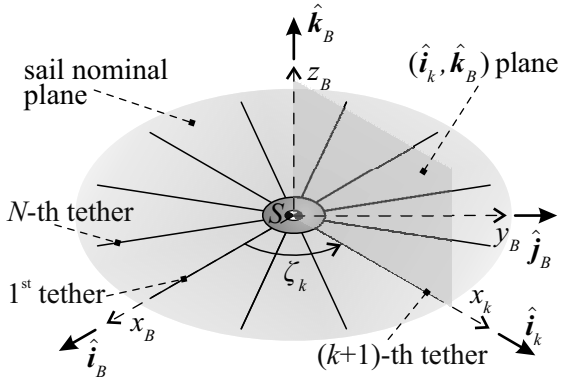

Figure 1. E-sail geometrical arrangement. Adapted from Ref. [10].

The E-sail consists of an even number $N \geq 4$ of tethers, each one denoted by a subscript k, with $k \in \{0,\, 1,\, \ldots,\, (N-1)\}$. The angular position of the k-th tether, measured counterclockwise on the $(x_B,\, y_B)$ plane starting from x_B, is given by

the azimuth angle

$$\zeta_k \triangleq \left(\frac{2\pi}{N}\right) k \tag{1}$$

Let $\hat{\boldsymbol{r}}$ be the local Sun-spacecraft unit vector, which approximately coincides with the direction of the solar wind velocity. The spacecraft orientation is defined by the sail pitch angle $\alpha_n \in [0,\, \pi/2]$ rad, that is, the angle between $\hat{\boldsymbol{r}}$ and the symmetry axis z_B, and by the clock angle $\delta_n \in [0,\, 2\pi)$ rad, that is, the angle between x_B and the projection of $\hat{\boldsymbol{r}}$ on the sail nominal plane. With reference to Fig. 2, the two angles $\{\alpha_n,\, \delta_n\}$ are given by

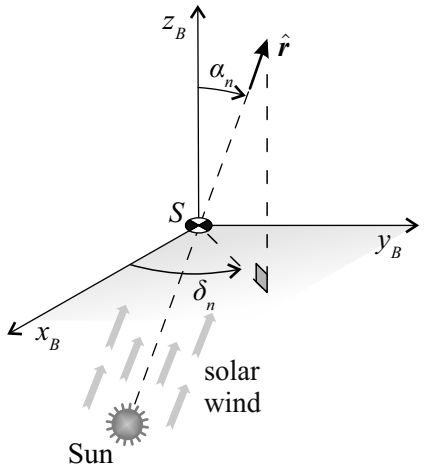

Figure 2. Pitch (α_n) and clock (δ_n) angles. Adapted from Ref. [26].

$$\alpha_n \triangleq \arccos(\hat{\boldsymbol{r}} \cdot \hat{\boldsymbol{k}}_B) \tag{2}$$

$$\delta_n \triangleq \begin{cases} \arccos\left(\dfrac{\hat{\boldsymbol{r}} \cdot \hat{\boldsymbol{i}}_B}{\|\hat{\boldsymbol{r}} \times \hat{\boldsymbol{k}}_B\|}\right) & \text{if } (\hat{\boldsymbol{r}} \cdot \hat{\boldsymbol{j}}_B) \geq 0 \\ 2\pi - \arccos\left(\dfrac{\hat{\boldsymbol{r}} \cdot \hat{\boldsymbol{i}}_B}{\|\hat{\boldsymbol{r}} \times \hat{\boldsymbol{k}}_B\|}\right) & \text{otherwise} \end{cases} \tag{3}$$

Note that δ_n is undefined when $\hat{\boldsymbol{k}}_B$ is parallel to $\hat{\boldsymbol{r}}$ and, as such, $\alpha_n = 0$. This special case is referred to as Sun-facing configuration [9].

Using a more accurate description of the actual E-sail shape [9], each tether bends on the $(x_k,\, z_B)$ plane as a consequence of the combined effects of the centrifugal force and the solar wind dynamic pressure acting on it, as is illustrated in Fig. 3. In particular, in a Sun-facing configuration the deformed tethers are well approximated by a natural logarithmic arc, whose analytical expression is

$$f = b_l\, L\, \ln\left(1 + \frac{x}{L}\right) \tag{4}$$

where f is the distance of the elementary length of tether (ds) from the $(x_B,\, y_B)$ plane, $x \in [0,\, L]$ is the distance of ds from z_B, and L is the tether length; see Fig. 3. In Eq. (4), the dimensionless shape coefficient b_l is given by

$$b_l \triangleq \frac{2\,\sigma\,u}{\rho\,\omega^2\,L} \tag{5}$$

where $u \simeq 400\,\mathrm{km/s}$ is the average solar wind speed, $\rho \simeq 10^{-5}\,\mathrm{kg/m}$ is the tether linear mass density [31], ω is the nominal sail spin rate. A compact expression for the design parameter σ when the Sun-spacecraft distance is about one astronomical unit [4, 28, 32] is given by

$$\sigma = 0.18\, \max(0,\, V - V_w)\, \sqrt{\epsilon_0\, m_p\, n} \tag{6}$$

in which V_w is the electrical potential of the solar wind ions (with an average value of 1 kV [4]), ϵ_0 the vacuum permittivity, m_p the proton mass, and n the local solar wind number density.

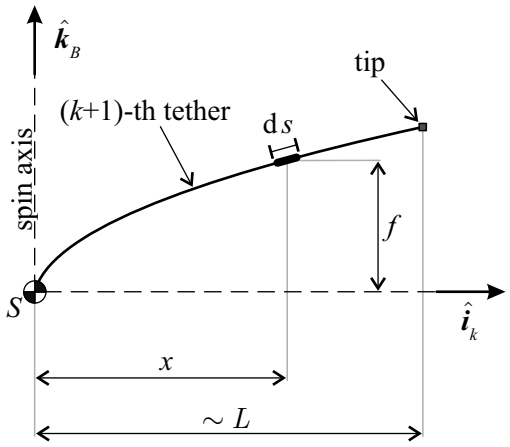

Figure 3. Tether deformed shape. Adapted from Ref. [26]

2.2 Torque vector model

The E-sail deformed shape induces the presence of a disturbance torque $\boldsymbol{T}_d$ to act on the spacecraft [9, 32]. Assuming all tethers to have the same electrical voltage V, such a disturbance torque may be written as [10]

$$\boldsymbol{T}_d = \frac{N\,L\,(\sigma\,u)^2\,\ln 2}{\rho\,\omega^2}\,(\hat{\boldsymbol{k}}_B \times \hat{\boldsymbol{r}}) \tag{7}$$

with

$$T_d \triangleq \|\boldsymbol{T}_d\| = \frac{N\,L\,(\sigma\,u)^2\,\ln 2}{\rho\,\omega^2}\,\sin\alpha_n \tag{8}$$

Note that the previous expression of $\boldsymbol{T}_d$ requires the spacecraft spin rate to be sufficiently high [9, 10] and, as such, the tether slope to be small, or

$$\max\left\{(f')^2\right\} = b_l^2 \simeq 0 \tag{9}$$

Moreover, the hypothesis of axially-symmetric E-sail is reasonable as long as its pitch angle does not exceed a few degrees [26]. The disturbance torque $\boldsymbol{T}_d$ may be counterbalanced with a modest modulation of the tether electrical voltage V by means of the design parameter σ. To that end, consider the plane, referred to as control plane, that passes

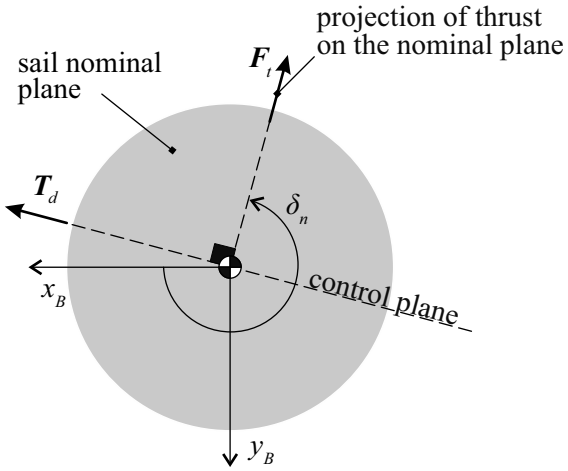

Figure 4. Disturbance torque and control plane trace.

through z_B and is parallel to $\boldsymbol{T}_d$; see Fig. 4. The control plane splits the E-sail in two parts characterized by two different levels of electrical potential. More precisely, the tethers belonging to the half-plane containing the projection of the thrust on the sail nominal plane ($\boldsymbol{F}_t$) are at a potential ($\sigma_{\max}$) higher than those belonging to the other half-plane ($\sigma_{\min}$). The two values of σ are [26]

$$\sigma_{\min} = \sigma - \frac{\Delta\sigma}{2} \quad , \quad \sigma_{\max} = \sigma + \frac{\Delta\sigma}{2} \tag{10}$$

where

$$\Delta\sigma \triangleq \ln(2)\, \sigma\, N\, \sin(\pi/N)\, b_l\, \tan\alpha_n \tag{11}$$

As long as $\Delta\sigma/\sigma \ll 1$, the assumption of axial symmetry may be retained even when the voltage of the two half-planes is (slightly) different. In that case, the required $\Delta\sigma$ per unit of generated torque is

$$\lambda \triangleq \frac{\Delta\sigma}{T_d} = \frac{2\, \sin(\pi/N)}{u\, L^2\, \cos\alpha_n} \tag{12}$$

Note that λ depends on the E-sail geometrical characteristics and on the actual sail attitude. Because λ is independent of the E-sail shape, a control torque obtained by individually modulating the tethers' voltage may be generated also in the special case of a flat E-sail.

Equation (12) will now be used to change the sail attitude and, at the same time, to remove the disturbance torque due to the tethers' bending.

3. Control law

The creation of a tangential thrust component requires the E-sail nominal plane to be oriented such as to reach a suitable value of the pitch angle. The aim of this section is to show how the spacecraft attitude may be adjusted with a control torque $\boldsymbol{T}_c$ generated through a suitable modulation of the tethers' electrical potential. Recall that the E-sail is assumed to maintain an axially-symmetric shape independent of the pitch angle α_n. The control torque $\boldsymbol{T}_c$ is the resultant of two vectors: 1) the attitude variation torque ($\boldsymbol{T}_a$), which ensures the required change of α_n to be obtained, and 2) the vector $-\boldsymbol{T}_d$, which removes the disturbance torque produced by the tethers' bending, that is

$$\boldsymbol{T}_c \triangleq \boldsymbol{T}_a - \boldsymbol{T}_d \tag{13}$$

The value of $\Delta\sigma$, necessary for generating the desired control torque $\boldsymbol{T}_c$, is obtained from Eq. (12) as

$$\Delta\sigma = \lambda\, T_c \tag{14}$$

where $T_c \triangleq \|\boldsymbol{T}_c\|$. The two vectors in Eq. (13) will now be analyzed separately.

Consider first the attitude variation torque. Its magnitude is found by enforcing a desired time evolution of the sail pitch angle. Without loss of generality, assume that the E-sail is initially placed in a Sun-facing configuration, such that its nominal plane is orthogonal to the Sun-sail direction. The attitude maneuver is better visualized with the aid of two additional reference frames. More precisely, let $\mathcal{T}_I(S;\, x_I,\, y_I,\, z_I)$ be an inertial reference frame of unit vectors $\{\hat{\boldsymbol{i}}_I,\, \hat{\boldsymbol{j}}_I,\, \hat{\boldsymbol{k}}_I\}$, where $\hat{\boldsymbol{i}}_I \equiv \hat{\boldsymbol{i}}_B(t=0)$ and $\hat{\boldsymbol{k}}_I \equiv \hat{\boldsymbol{k}}_B(t=0) \equiv \hat{\boldsymbol{r}}$. Introduce also an auxiliary reference frame $\mathcal{T}_A(S;\, x_A,\, y_A,\, z_A)$ of unit vectors $\{\hat{\boldsymbol{i}}_A,\, \hat{\boldsymbol{j}}_A,\, \hat{\boldsymbol{k}}_A\}$, where $\hat{\boldsymbol{j}}_A \equiv \hat{\boldsymbol{j}}_I$. The latter is a non-inertial reference frame, which rotates about the y_A-axis (fixed in the inertial space) of an angle equal to the pitch angle α_n, until the attitude reorientation maneuver is completed; see Fig. 5. The rotation of the sail nominal plane is chosen to track a desired time variation of the pitch angle, that is

$$\dot{\widetilde{\alpha}}_n \triangleq A \left[1 - \frac{4}{t_f^2} \left(t - \frac{t_f}{2} \right)^2 \right] \tag{15}$$

where the symbol $\widetilde{\square}$ denotes the desired value, t is the time, t_f the maneuver time, and A is a suitable constant. Note that the initial and final equilibrium conditions at the beginning and at the end of the maneuver, that is, $\dot{\widetilde{\alpha}}_n(0) = \dot{\widetilde{\alpha}}_n(t_f) = 0$, are automatically met. The integral of Eq. (15) is

$$\widetilde{\alpha}_n = \int_0^t A \left[1 - \frac{4}{t_f^2} \left(\xi - \frac{t_f}{2} \right)^2 \right] \mathrm{d}\xi = \frac{2\, A}{t_f} \left(t^2 - \frac{2}{3} \frac{t^3}{t_f} \right) \tag{16}$$

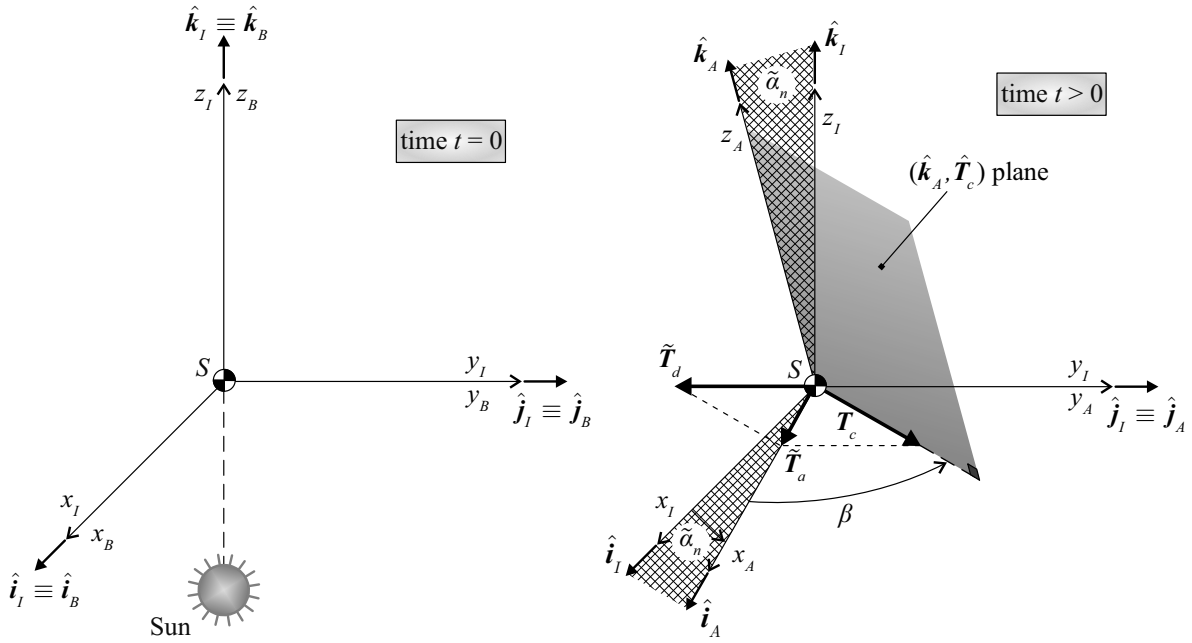

(a) E-sail orientation at $t = 0$.

(b) Attitude maneuver.

Figure 5. Sketch of the attitude maneuver with the control torque.

while A may be calculated by enforcing the final condition $\widetilde{\alpha}_n(t_f) \triangleq \widetilde{\alpha}_{n_f}$, that is

$$A = \frac{3\,\widetilde{\alpha}_{n_f}}{2\,t_f} \tag{17}$$

from which

$$\dot{\widetilde{\alpha}}_n = \frac{6\,\widetilde{\alpha}_{n_f}}{t_f}\left[\frac{t}{t_f} - \left(\frac{t}{t_f}\right)^2\right] \tag{18}$$

The attitude variation torque $\boldsymbol{T}_a$ is chosen such that the rate of change of α_n equals that given by Eq. (18). Let $\boldsymbol{\Omega}_A$ be the angular velocity with which the auxiliary frame $\mathcal{T}_A$ rotates about its y_A-axis, such that $\boldsymbol{\Omega}_A = \dot{\widetilde{\alpha}}_n\,\hat{\boldsymbol{j}}_A$. If the sail pitch angle were able to meet the desired time variation of Eq. (16), the principal body frame would exactly follow the auxiliary frame during the whole maneuver and, accordingly, the E-sail spin axis z_B would always coincide with z_A. The (constant) components of the desired spacecraft angular momentum vector $\widetilde{\boldsymbol{H}}$ in the auxiliary frame are therefore $\widetilde{\boldsymbol{H}} = I_z\,\omega\,\hat{\boldsymbol{k}}_A$, where I_z is the spacecraft longitudinal moment of inertia. The required attitude variation torque $\widetilde{\boldsymbol{T}}_a$ is given by

$$\widetilde{\boldsymbol{T}}_a = \boldsymbol{\Omega}_A \times \widetilde{\boldsymbol{H}} = T_a\,\hat{\boldsymbol{i}}_A \tag{19}$$

where $T_a \triangleq \|\widetilde{\boldsymbol{T}}_a\|$, with

$$T_a \triangleq I_z\,\omega\,\dot{\widetilde{\alpha}}_n = \frac{6\,\widetilde{\alpha}_{n_f}\,I_z\,\omega}{t_f}\left[\frac{t}{t_f} - \left(\frac{t}{t_f}\right)^2\right] \tag{20}$$

Moreover, under the previous assumption that $z_B \equiv z_A$, the onset of a pitch angle different from zero also causes a disturbance torque to act along the y_A-axis, that is, $\widetilde{\boldsymbol{T}}_d = -T_d\,\hat{\boldsymbol{j}}_A$, where T_d is given by Eq. (8). From Eq. (13) the control torque is

$$\boldsymbol{T}_c \simeq \widetilde{\boldsymbol{T}}_a - \widetilde{\boldsymbol{T}}_d \tag{21}$$

or

$$\boldsymbol{T}_c \simeq \frac{6\,\widetilde{\alpha}_{n_f}\,I_z\,\omega}{t_f}\left[\frac{t}{t_f} - \left(\frac{t}{t_f}\right)^2\right]\hat{\boldsymbol{i}}_A + \frac{N\,L\,(\sigma\,u)^2\,\ln 2}{\rho\,\omega^2}\,\sin\alpha_n\,\hat{\boldsymbol{j}}_A \tag{22}$$

While the attitude variation torque $\widetilde{\boldsymbol{T}}_a$ is an explicit function of time, $\widetilde{\boldsymbol{T}}_d$ depends on α_n, which must therefore be measured during the maneuver. Because $\widetilde{\boldsymbol{T}}_a$ and $\widetilde{\boldsymbol{T}}_d$ are perpendicular vectors, the magnitude of the control torque is

$$T_c \triangleq \|\boldsymbol{T}_c\| = \sqrt{\frac{36\,\widetilde{\alpha}_{n_f}^2\, I_z^2\,\omega^2}{t_f^2}\left[\frac{t}{t_f}-\left(\frac{t}{t_f}\right)^2\right]^2+\frac{N^2\,L^2\,(\sigma\,u)^4\,(\ln 2)^2}{\rho^2\,\omega^4}\,\sin^2\alpha_n} \tag{23}$$

In analogy with the previously described approach for counterbalancing the disturbance torque alone, the E-sail fundamental plane is now split in two parts by the control plane, which is orthogonal to the $(x_A,\ y_A)$ plane and passes through $\boldsymbol{T}_c$. Again, the tethers belonging to the half-planes separated by the control plane are set to two different levels of electrical potential, that is, according to Eq. (14), $\sigma \pm \lambda\, T_c/2$. The orientation of the control plane is defined by $\beta = \beta(t, \alpha_n) \in [0,\ 2\pi)$, which is the angle between $\boldsymbol{T}_c$ and the x_A-axis, measured counterclockwise from x_A. With reference to Fig. 6, β is obtained as

$$\beta \triangleq \arctan\left(\frac{T_d}{T_a}\right) \tag{24}$$

where T_d and T_a are given by Eqs. (8) and (20), respectively. Note that when the maneuver ends, $T_a \to 0$ and $\beta \to \pi/2$.

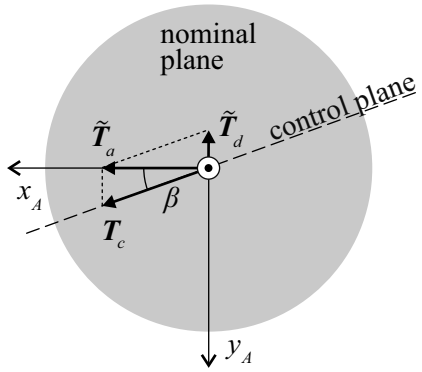

Figure 6. Control torque and orientation of the control plane trace.

The value of σ_k to be assigned to each tether depends on the angular displacement γ_k of the generic tether relative to the control plane, that is

$$\gamma_k \triangleq \omega\, t + \zeta_k - \beta \tag{25}$$

The resultant control law is therefore

$$\sigma_k = \begin{cases} \sigma - \lambda\,\dfrac{T_c}{2} & \text{if} \quad \gamma_k \in [0,\ \pi)\,\text{rad} \\ \sigma + \lambda\,\dfrac{T_c}{2} & \text{if} \quad \gamma_k \in [\pi,\ 2\pi)\,\text{rad} \end{cases} \tag{26}$$

where σ is given by Eq. (6), λ is obtained from Eq. (12), and T_c from Eq. (23). Finally, β is given by

$$\beta = \begin{cases} \arctan\left(\dfrac{T_d}{T_a}\right) & \text{if} \quad t \le t_f \\ \dfrac{\pi}{2}\,\text{rad} & \text{if} \quad t > t_f \end{cases} \tag{27}$$

4. Numerical simulations

The effectiveness of the previous control law is now checked by numerically integrating the Euler's attitude equations. To that end, the torque components generated by the E-sail are written in the principal body frame $\mathcal{T}_B$. Let $\{\phi,\ \theta,\ \psi\}$ be

the Euler's angles that define the orientation of $\mathcal{T}_B$ with respect to the inertial reference frame. Using the rotational sequence $3(\psi) \rightarrow 1(\phi) \rightarrow 2(\theta)$ [33] to describe the orientation of $\mathcal{T}_B$ relative to $\mathcal{T}_I$, the kinematic equations of a rigid E-sail-based spacecraft are [26]

$$\dot{\phi} = \Omega_x \, \cos\theta + \Omega_z \, \sin\theta \tag{28}$$

$$\dot{\theta} = \Omega_y - (\Omega_z \, \cos\theta - \Omega_x \, \sin\theta) \, \tan\phi \tag{29}$$

$$\dot{\psi} = (\Omega_z \, \cos\theta - \Omega_x \, \sin\theta) \, \sec\phi \tag{30}$$

where $[\boldsymbol{\Omega}]_{\mathcal{T}_B} \triangleq [\Omega_x \; \Omega_y \; \Omega_z]^{\mathrm{T}}$ are the angular velocity components of the spacecraft. The pitch and clock angles are related to the Euler's angles as

$$\cos\alpha_n = \cos\phi \, \cos\theta \tag{31}$$

$$\sin\alpha_n \, \sin\delta_n = \sin\phi \tag{32}$$

$$\sin\alpha_n \, \cos\delta_n = -\cos\phi \, \sin\theta \tag{33}$$

The Euler's equations may be written as [26]

$$\dot{\Omega}_x = \frac{I_t - I_z}{I_t} \, \Omega_y \, \Omega_z + \frac{\mathcal{E}}{I_t} \tag{34}$$

$$\dot{\Omega}_y = \frac{I_z - I_t}{I_t} \, \Omega_x \, \Omega_z + \frac{\mathcal{F}}{I_t} \tag{35}$$

$$\dot{\Omega}_z = \frac{\mathcal{G}}{I_z} \tag{36}$$

where I_t is the spacecraft transverse moment of inertia, while $\mathcal{E}$, $\mathcal{F}$, and $\mathcal{G}$ are the components of the total torque generated by the E-sail in the principal body frame. Note that $\{\mathcal{E}, \, \mathcal{F}, \, \mathcal{G}\}$ not only include the contribution to the total torque given by the modulation of the electrical voltage, but also the effects of tethers' bending. As is shown in Ref. [26], the components of the total torque can be written as

$$\mathcal{E} \triangleq \sum_{k=0}^{N-1} \mathcal{E}_k \quad , \quad \mathcal{F} \triangleq \sum_{k=0}^{N-1} \mathcal{F}_k \quad , \quad \mathcal{G} \triangleq \sum_{k=0}^{N-1} \mathcal{G}_k \tag{37}$$

where

$$\mathcal{E}_k \triangleq \int_0^L \mathrm{d}\mathcal{E}_k \quad , \quad \mathcal{F}_k \triangleq \int_0^L \mathrm{d}\mathcal{F}_k \quad , \quad \mathcal{G}_k \triangleq \int_0^L \mathrm{d}\mathcal{G}_k \tag{38}$$

are the components of the total torque provided by the k-th tether. The complete expressions of $\mathrm{d}\mathcal{E}_k$, $\mathrm{d}\mathcal{F}_k$, and $\mathrm{d}\mathcal{G}_k$, taken from Ref. [26], are reported below for the sake of completeness under the assumption that $(f')^2 \simeq 0$ (see Eq.(9))

$$\mathrm{d}\mathcal{E}_k = \{x \, \sin\zeta_k \, [\sigma_k \, u \, \cos\alpha_n - f' \, \sigma_k \, u \sin\alpha_n \, \cos(\delta_n - \zeta_k)] - f \, \sigma_k \, u \, \sin\alpha_n \, \sin\delta_n +$$

$$- f \, \sin\zeta_k \, \left[\rho \, x \, \omega^2 - \sigma_k \, u \, (\sin\alpha_n \, \cos(\delta_n - \zeta_k) + f' \, \cos\alpha_n)\right]\} \, \mathrm{d}x \tag{39}$$

$$\mathrm{d}\mathcal{F}_k = \{-x \, \cos\zeta_k \, [\sigma_k \, u \, \cos\alpha_n - f' \, \sigma_k \, u \sin\alpha_n \, \cos(\delta_n - \zeta_k)] + f \, \sigma_k \, u \, \sin\alpha_n \, \cos\delta_n +$$

$$+ f \, \cos\zeta_k \, \left[\rho \, x \, \omega^2 - \sigma_k \, u \, (\sin\alpha_n \, \cos(\delta_n - \zeta_k) + f' \, \cos\alpha_n)\right]\} \, \mathrm{d}x \tag{40}$$

$$\mathrm{d}\mathcal{G}_k = \sigma_k \, u \, x \, \sin\alpha_n \, \sin(\delta_n - \zeta_k) \, \mathrm{d}x \tag{41}$$

The torque components from the k-th tether are obtained by integrating Eqs. (39)–(41) along the tether length and recalling that $b_l^2 \simeq 0$. The result is

$$\mathcal{E}_k = L^2\,\sigma_k\,u\,\left\{\frac{\cos\alpha_n\,\sin\zeta_k}{2}\,\left(1-\frac{\sigma}{\sigma_k\,\cos\alpha_n}\right)+b_l\,\sin\alpha_n\,\left[\cos(\delta_n-\zeta_k)\,\sin\zeta_k\,(\ln 8-2)-\sin\delta_n\,(\ln 4-1)\right]\right\} \quad (42)$$

$$\mathcal{F}_k = L^2\,\sigma_k\,u\,\left\{\frac{\cos\alpha_n\,\cos\zeta_k}{2}\,\left(\frac{\sigma}{\sigma_k\,\cos\alpha_n}-1\right)-b_l\,\sin\alpha_n\,\left[\cos(\delta_n-\zeta_k)\,\cos\zeta_k\,(\ln 8-2)-\cos\delta_n\,(\ln 4-1)\right]\right\} \quad (43)$$

$$\mathcal{G}_k = \frac{L^2\,\sigma_k\,u\,\sin(\delta_n-\zeta_k)\,\sin\alpha_n}{2} \quad (44)$$

For exemplary purposes assume that $I_z = 6\,I_t = 1000\,\mathrm{kg\,m^2}$, $N = 500$, $L = 2000\,\mathrm{km}$, and $\omega \simeq 0.0758\,\mathrm{rad/s}$, from which $b_l \simeq 0.0065$. The initial conditions are $\phi(0) = \theta(0) = \psi(0) = \Omega_x(0) = \Omega_y(0) = 0$ and $\omega(0) = \omega$. The equations of motion (28)–(36) have been numerically integrated by implementing the control law (26)–(27) when $\widetilde{\alpha}_{n_f} = 5\,\mathrm{deg}$ and $t_f = 2\,\mathrm{minutes}$. The simulations are reported in a time span equal to $2\,t_f$ to verify whether the E-sail is able to maintain its final attitude with the proposed control law. The results are shown in Figs. 7–8. The time evolution of the sail pitch angle during and after the attitude maneuver (see Fig. 7) exhibits an oscillatory behavior around an average value of about 4.95 deg, which is close to the desired angle of 5 deg. The mean asymptotic value tends to slightly decrease over time. Such a behavior is due to the generation of a torque along the z_B-axis, which causes a small variation of the sail spin rate from 0.0758 rad/s to 0.0761 rad/s; see Eq. (36) and Fig. 8. Notably, in the case when the torque along z_B is set equal to zero, the observed decrease of α_n no longer occurs. The $\mathcal{G}$ component could therefore be removed by suitably adjusting the spacecraft spin rate. Figure 8 also shows the components $\mathcal{E}$ and $\mathcal{F}$, whose values never exceed 0.5 N m. Finally, Fig. 9 reports the time evolution of the maximum and minimum values of σ_k/σ. Recall that $\sigma_{\max}(0) = \sigma_{\min}(0) = \sigma$ because the E-sail starts from a Sun-facing configuration. During the attitude change, the maximum (minimum) value of σ_k/σ is about 1.0021 (0.9979). This means that the tether electrical voltage requires a very small variation, which is less than 0.22% with respect to its nominal value. The values of σ_k for $t > t_f$ allow the E-sail to maintain the final attitude, in accordance with the results presented in Ref. [26].

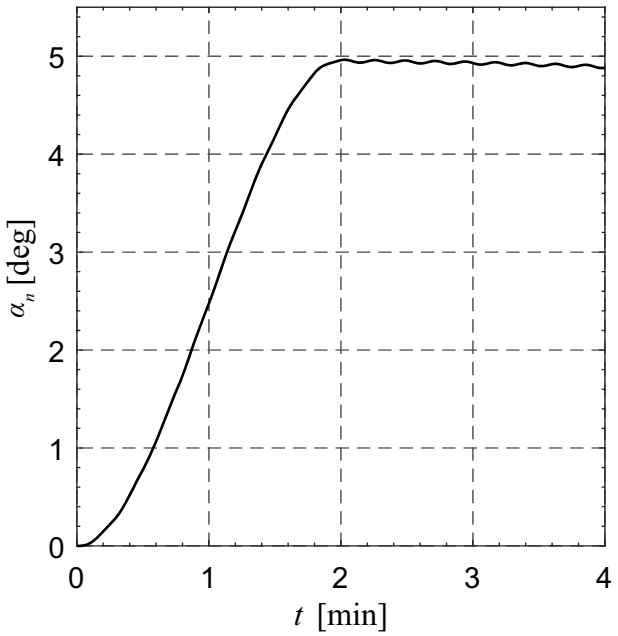

Figure 7. Evolution of α_n during attitude maneuver and maintenance.

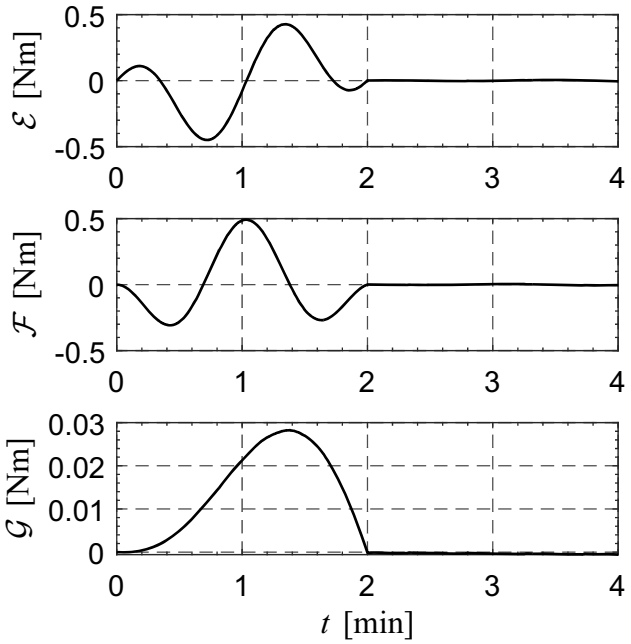

Figure 8. Components of E-sail torque in $\mathcal{T}_B$ during attitude maneuver and maintenance.

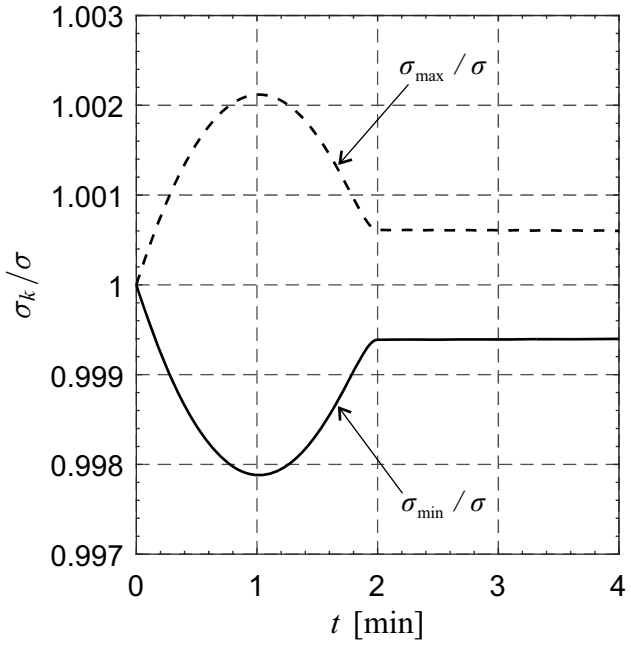

Figure 9. Maximum and minimum values of σ_k/σ during attitude maneuver and maintenance.

5. Conclusions

The attitude of an E-sail-based spacecraft may be changed by individually modulating the electrical voltage of the tethers. To that end, an analytical control law has been derived, in which the voltage level of each tether is expressed as a function of time and current sail pitch angle. It has been shown that a small variation of the voltage level is sufficient for most practical purposes. The proposed method for controlling and maintaining the spacecraft attitude is easy to implement and offer good performance in terms of attitude reorientation time. The numerical simulations have shown that an attitude change induces the onset of a torque along the spacecraft symmetry axis, which is responsible of a small variation of the sail spin rate. As a result, at the end of the maneuver the pitch angle is not maintained at a constant value, but tends to slowly decrease over time. Such an unwanted phenomenon is instead absent in the case when the torque along the symmetry axis is set equal to zero. A possible solution is therefore to compensate the decrease of the sail spin rate.

A natural extension of this work is the analysis of the performance sensitivity to the design parameters, such as the maneuver time or the spacecraft moments of inertia. Moreover, the control law may be refined to maintain the target attitude with a more accuracy level.

References

[1] Janhunen, P., "Electric sail for spacecraft propulsion," *Journal of Propulsion and Power*, Vol. 20, No. 4, 2004, pp. 763–764. doi:10.2514/1.8580.

[2] Janhunen, P., and Sandroos, A., "Simulation study of solar wind push on a charged wire: basis of solar wind electric sail propulsion," *Annales Geophysicae*, Vol. 25, No. 3, 2007, pp. 755–767. doi:10.5194/angeo-25-755-2007.

[3] Janhunen, P., "Status report of the electric sail in 2009," *Acta Astronautica*, Vol. 68, No. 5-6, 2011, pp. 567–570. doi: 10.1016/j.actaastro.2010.02.007.

[4] Janhunen, P., Toivanen, P. K., Polkko, J., Merikallio, S., Salminen, P., Haeggström, E., Seppänen, H., Kurppa, R., Ukkonen, J., Kiprich, S., Thornell, G., Kratz, H., Richter, L., Krömer, O., Rosta, R., Noorma, E. J., M. and, Lätt, S., Mengali, G., Quarta, A. A., Koivisto, H., Tarvainen, O., Kalvas, T., Kauppinen, J., Nuottajärvi, A., and Obraztsov, A., "Invited article: Electric solar wind sail: toward test missions," *Review of Scientific Instruments*, Vol. 81, No. 11, 2010, pp. 111301–1–11301–11. doi:10.1063/1.3514548.

[5] Janhunen, P., Quarta, A. A., and Mengali, G., "Electric solar wind sail mass budget model," *Geoscientific Instrumentation, Methods and Data Systems*, Vol. 2, No. 1, 2013, pp. 85–95. doi:10.5194/gi-2-85-2013.

[6] Fulton, J., and Schaub, H., "Fixed-axis electric sail deployment dynamics analysis using hub-mounted momentum control," *Acta Astronautica*, Vol. 144, 2018, pp. 160–170. doi:10.1016/j.actaastro.2017.11.048.

[7] Quarta, A. A., and Mengali, G., "Minimum-time trajectories of electric sail with advanced thrust model," *Aerospace Science and Technology*, Vol. 55, 2016, pp. 419–430. doi:10.1016/j.ast.2016.06.020.

[8] Huo, M., Mengali, G., and Quarta, A. A., "Electric sail thrust model from a geometrical perspective," *Journal of Guidance, Control, and Dynamics*, Vol. 41, No. 3, 2018, pp. 735–741. doi:10.2514/1.G003169.

[9] Bassetto, M., Mengali, G., and Quarta, A. A., "Thrust and torque vector characteristics of axially-symmetric E-sail," *Acta Astronautica*, Vol. 146, 2018, pp. 134–143. doi:10.1016/j.actaastro.2018.02.035.

[10] Bassetto, M., Mengali, G., and Quarta, A. A., "Stability and control of spinning E-sail in heliostationary orbit," *Journal of Guidance, Control, and Dynamics*, Vol. 42, No. 2, 2018, pp. 425–431. doi:10.2514/1.G003788.

[11] Mengali, G., Quarta, A. A., and Aliasi, G., "A graphical approach to electric sail mission design with radial thrust," *Acta Astronautica*, Vol. 82, No. 2, 2013, pp. 197–208. doi:10.1016/j.actaastro.2012.03.022.

[12] Quarta, A. A., and Mengali, G., "Analysis of electric sail heliocentric motion under radial thrust," *Journal of Guidance, Control, and Dynamics*, Vol. 39, No. 6, 2016, pp. 1431–1435. doi:10.2514/1.G001632.

[13] Quarta, A. A., and Mengali, G., "Optimal Solar Sail Transfer to Linear Trajectories," *Acta Astronautica*, Vol. 82, No. 2, 2013, pp. 189–196. doi:10.1016/j.actaastro.2012.03.005.

[14] Niccolai, L., Quarta, A. A., and Mengali, G., "Electric sail-based displaced orbits with refined thrust model," *Proceedings of the Institution of Mechanical Engineers, Part G: Journal of Aerospace Engineering*, Vol. 232, No. 3, 2018, pp. 423–432. doi:10.1177/0954410016679195.

[15] Niccolai, L., Quarta, A. A., and Mengali, G., "Electric sail elliptic displaced orbits with advanced thrust model," *Acta Astronautica*, Vol. 138, 2017, pp. 503–511. doi:10.1016/j.actaastro.2016.10.036.

[16] Quarta, A. A., and Mengali, G., "Electric sail missions to potentially hazardous asteroids," *Acta Astronautica*, Vol. 66, No. 9-10, 2010, pp. 1506–1519. doi:10.1016/j.actaastro.2009.11.021.

[17] Quarta, A. A., Mengali, G., and Janhunen, P., "Electric sail for a near-Earth asteroid sample return mission: case 1998 KY26," *Journal of Aerospace Engineering*, Vol. 27, No. 6, 2014. doi:10.1061/(ASCE)AS.1943-5525.0000285.

[18] Mengali, G., and Quarta, A. A., "Optimal nodal flyby with near-Earth asteroids using electric sail," *Acta Astronautica*, Vol. 104, No. 2, 2014, pp. 450–457. doi:10.1016/j.actaastro.2014.02.012.

[19] Quarta, A. A., Mengali, G., and Janhunen, P., "Electric sail option for cometary rendezvous," *Acta Astronautica*, Vol. 127, 2016, pp. 684–692. doi:10.1016/j.actaastro.2016.06.020.

[20] Janhunen, P., Merikallio, S., and Paton, M., "EMMI - Electric solar wind sail facilitated Manned Mars Initiative," *Acta Astronautica*, Vol. 113, 2015, pp. 22–28. doi:10.1016/j.actaastro.2015.03.029.

[21] Janhunen, P., and Toivanen, P. K., "Safety criteria for flying E-sail through solar eclipse," *Acta Astronautica*, Vol. 114, 2015, pp. 1–5. doi:10.1016/j.actaastro.2015.04.006.

[22] Bassetto, M., Quarta, A. A., and Mengali, G., "Locally-Optimal Electric Sail Transfer," *Proceedings of the Institution of Mechanical Engineers, Part G: Journal of Aerospace Engineering,*, Vol. 233, No. 1, 2019, pp. 166–179. doi:10.1177/0954410017728975.

[23] Mengali, G., Quarta, A. A., and Janhunen, P., "Considerations of electric sailcraft trajectory design," *Journal of the British Interplanetary Society*, Vol. 61, No. 8, 2008, pp. 326–329.

[24] Quarta, A. A., and Mengali, G., "Electric sail mission analysis for outer solar system exploration," *Journal of Guidance, Control, and Dynamics*, Vol. 33, No. 3, 2010, pp. 740–755. doi:10.2514/1.47006.

[25] Janhunen, P., Lebreton, J.-P., Merikallio, S., Paton, M., Mengali, G., and Quarta, A. A., "Fast E-sail Uranus entry probe mission," *Planetary and Space Science*, Vol. 104, 2014, pp. 141–146. doi:10.1016/j.pss.2014.08.004.

[26] Bassetto, M., Mengali, G., and Quarta, A. A., "Attitude dynamics of an electric sail model with a realistic shape," *Acta Astronautica*, Vol. 159, 2019, pp. 250–257. doi:10.1016/j.actaastro.2019.03.064.

[27] Janhunen, P., "Photonic spin control for solar wind electric sail," *Acta Astronautica*, Vol. 83, 2013, pp. 85–90. doi:10.1016/j.actaastro.2012.10.017.

[28] Toivanen, P. K., and Janhunen, P., "Spin plane control and thrust vectoring of electric solar wind sail," *Journal of Propulsion and Power*, Vol. 29, No. 1, 2013, pp. 178–185. doi:10.2514/1.B34330.

[29] Toivanen, P. K., Janhunen, P., and Envall, J., "Electric sail control mode for amplified transverse thrust," *Acta Astronautica*, Vol. 106, 2015, pp. 111–119. doi:10.1016/j.actaastro.2014.10.031.

[30] Janhunen, P., and Toivanen, P. K., "A scheme for controlling the E-sail's spin rate by the E-sail effect itself," *Space Propulsion 2018*, Seville, Spain, 2018.

[31] Seppänen, H., Rauhala, T., Kiprich, S., Ukkonen, J., Simonsson, M., Kurppa, R., Janhunen, P., and Hæggström, E., "One kilometer (1 km) electric solar wind sail tether produced automatically," *Review of Scientific Instruments*, Vol. 84, No. 9, 2013. doi:10.1063/1.4819795.

[32] Toivanen, P. K., and Janhunen, P., "Thrust vectoring of an electric solar wind sail with a realistic sail shape," *Acta Astronautica*, Vol. 131, 2017, pp. 145–151. doi:10.1016/j.actaastro.2016.11.027.

[33] Wertz, J. R. (ed.), *Spacecraft Attitude Determination and Control*, 1st ed., Astrophysics and Space Science Library, Springer Netherlands, Dordrecht, Holland, 1978, pp. 760–766. doi:10.1007/978-94-009-9907-7.